Cross-shore sediment transport and the equilibrium morphology of mudflats under tidal currents

D. Pritchard

B. P. Institute for Multiphase Flow, University of Cambridge, Cambridge, UK

A. J. Hogg

Centre for Environmental and Geophysical Flows, Department of Mathematics, University of Bristol, Bristol, UK

Received 29 July 2002; accepted 29 July 2003; published 8 October 2003.

[1] We describe a mathematical model of suspended sediment transport under cross-shore tidal currents on an intertidal mudflat. We employ a Lagrangian formulation to obtain periodic solutions for the sediment transport over idealized bathymetries and use these to investigate the process of settling lag. In deep water away from the shoreline the concentration of suspended sediment tends to a constant value, and we may invert the relation between bathymetry and offshore concentration to estimate how the gradient of a flat in a state of equilibrium varies with the sediment properties and supply. These analytical estimates are compared successfully with the numerical experiments of previous studies. We discuss the robustness of our modeling framework and demonstrate its application to different descriptions of sediment transport and tidal regimes. *INDEX TERMS:* 3020 Marine Geology and Geophysics: Littoral processes; 3022 Marine Geology and Geophysics: Marine sediments—processes and transport; 4235 Oceanography: General: Estuarine processes; 4546 Oceanography: Physical: Nearshore processes; 4558 Oceanography: Physical: Sediment transport;
KEYWORDS: estuaries, intertidal mudflats, intertidal sedimentation, mathematical models, morphodynamics

Citation: Pritchard, D., and A. J. Hogg, Cross-shore sediment transport and the equilibrium morphology of mudflats under tidal currents, *J. Geophys. Res.*, *108*(C10), 3313, doi:10.1029/2002JC001570, 2003.

1. Introduction

[2] Intertidal mudflats, extensive coastal regions dominated by fine cohesive sediment, are found throughout the world, wherever there is a sufficient supply of sediment [*Flemming*, 2002]. They are characterized by extremely low gradients, leading to a tidal incursion of as much as several kilometers, and are often backed by low-lying saltmarsh regions; they form an especially important environment along the coasts of northwestern Europe, including the British Isles, where they dominate the shores of many estuaries.

[3] Mudflats provide a habitat for many species of wading birds, and are economically important through their role in coastal defense and as a substantial sink or source of sediment during engineering works [*Roberts and Whitehouse*, 1997]. However, the morphodynamics of muddy shores have been rather less studied than those of sandy beaches. It is only in the last decade that large programmes of field work have started to clarify the properties of the sediment, the mechanisms by which it is transported, and how the flat morphology varies with factors such as the tidal regime and the sediment properties and supply. In particular, the work carried out under the European Commission's INTRMUD project has provided for the first time a substantial set of data on European mudflats (see the special edition of *Continental Shelf Research*, 20, 10–13, 2000). A number of systematic studies [*Kirby*, 1992; *Dyer*, 1998; *Kirby*, 2000] have drawn on these and other observations to identify the environmental factors which exert most influence on the evolution of mudflats, and to characterize the morphologies which develop under given conditions.

[4] *Kirby* [2000] found that the cross-shore profiles of mudflats can be characterized by the relative contributions made by wind-generated waves and tidal currents to the total sediment transport. Flats dominated by waves tend to have a concave upward profile and to retreat over decadal timescales, while those dominated by tidal currents are convex upward and accrete over decadal timescales.

[5] This paper is concerned with flats which evolve under purely tidal forcing. Most mudflats, with the possible exception of those in extremely sheltered estuarine environments, are influenced both by tidal currents and by the action of surface waves [*Le Hir et al.*, 2000]. However, this idealization allows us to make significant progress in characterizing the transport processes, and this provides a starting point for understanding the dynamics of flats under more complex hydrodynamic conditions. Our approach throughout is to consider the simplest model which yields physical insight: hence, for example, we neglect processes such as the diffusion of suspended sediment and the effect of wave stresses on the properties of the bed.

[6] Previous modeling studies of tidally dominated flats have been carried out both analytically [*Friedrichs and Aubrey*, 1996] and numerically [*Roberts et al.*, 2000;

0148-0227/03/2002JC001570$09.00

Pritchard et al., 2002], while reviews on the issues involved have been provided for wave-dominated flats by *Lee and Mehta* [1997] and more generally by *Le Hir et al.* [2000]. These studies are briefly summarized in section 2.2. The object of the current paper is to develop an analytical framework, building on that of *Friedrichs and Aubrey* [1996], within which sediment transport may be described and the resulting equilibrium morphology predicted. These predictions then allow estimates of the equilibrium states to be made without the need for extensive computations, and so provide a bridge between existing analytical and numerical results.

[7] In section 2, we describe a framework for modeling morphodynamic processes, incorporating the cross-shore hydrodynamics and the transport of fine sediment in suspension, and briefly review previous studies. In section 3, we consider sediment transport in a Lagrangian formulation, using the method described in Appendix A. We construct analytical and numerical solutions for periodic transport over idealized bathymetries, and consider in some detail the processes of net sediment transport which they reveal. In particular, we discuss the roles of settling and scour lag in this hydrodynamic setting. These results provide the basis for section 4, in which we use them to develop estimates for the large-scale morphology of the flat; these estimates are compared with the numerical results of *Pritchard et al.* [2002] and of *Roberts et al.* [2000], and we discuss their application in the field.

[8] In two appendices, we investigate the robustness of these results to uncertainties in the sediment transport model. In Appendix B, we consider more general models for the erosion and deposition of suspended sediment, and demonstrate that the principal features of our results remain unchanged. In Appendix C, we examine the sensitivity of our estimates to uncertainties in the sediment properties, and its implications both for our own and for related modeling approaches.

2. Description of the Model

[9] We employ a depth-integrated "shallow-water" model for hydrodynamics and sediment transport, of the kind which have become an established tool in both engineering and geophysical studies of coastal and estuarine systems [see, e.g., *Friedrichs et al.*, 1998; *Brenon and Le Hir*, 1999; *Schuttelaars and de Swart*, 1999; *Roberts et al.*, 2000; *Wood and Widdows*, 2002]. These models are known to provide a useful source of geophysical insight, although considerable "tuning" is often required when they are used for predictive purposes. In order to obtain clearer insight into the dominant physical processes, we have simplified the descriptions of both the hydrodynamics and the sediment dynamics as far as possible while retaining the essential physics of the system.

2.1. Model Geometry and Governing Equations

[10] The geometry of the cross-shore model is shown in Figure 1, which illustrates a prototypical macrotidal flat. We consider forcing solely by cross-shore tidal currents, noting that it is only in deeper water that longshore flows may be expected to dominate the sediment transport [*Le Hir et al.*, 2000].

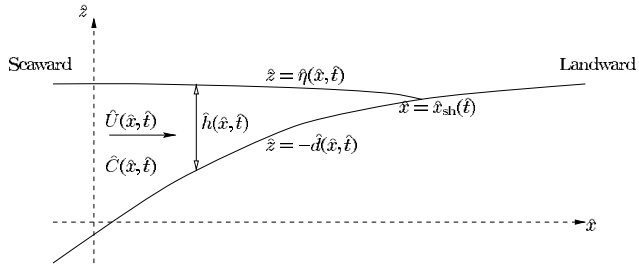

Figure 1. Definition diagram for cross-shore model (vertically exaggerated for clarity).

[11] The water depth is denoted by $\hat{h}(\hat{x}, \hat{t})$, bed elevation by $\hat{z} = -\hat{d}(\hat{x}, \hat{t})$ and water surface elevation by $\hat{z} = \hat{\eta}(\hat{x}, \hat{t}) = \hat{h} - \hat{d}$, and the instantaneous shoreline position is denoted by $\hat{x} = \hat{x}_{sh}(\hat{t})$. (Throughout this paper, carets ^ denote dimensional variables, while dimensionless variables are unadorned.)

[12] We describe the fluid velocity and the mass concentration of suspended sediment (SSC) in terms of depth-averaged quantities $\hat{U}(\hat{x}, \hat{t})$ and $\hat{C}(\hat{x}, \hat{t})$. This depth-averaged approach is appropriate when the characteristic vertical length scale of the flow is very much smaller than the horizontal length scale [*Peregrine*, 1972]. Since the typical gradients of intertidal flats are of the order of 1/100 or smaller [*Dyer et al.*, 2000b], this condition is well satisfied for the large-scale properties of the flow.

[13] It is convenient to work in terms of the nondimensional variables defined by $x = \hat{x}/(\hat{U}_0\hat{T})$, $h = \hat{h}/\hat{\eta}_0$, $d = \hat{d}/\hat{\eta}_0$, $U = \hat{U}/\hat{U}_0$ and $C = \hat{C}/\hat{C}_0$, where $\hat{T}$ denotes the tidal period and $\hat{\eta}_0$ the tidal range, and $\hat{U}_0$ and $\hat{C}_0$ are scales of "typical" cross-shore velocity and SSC respectively. It is important to note that the horizontal length scale (and thus the gradient of the flat) is not set independently of $\hat{U}_0\hat{T}$, but emerges as a consequence of morphodynamic processes. Hence we may expect $\hat{U}_0$, as well as $\hat{C}_0$, to be related to the sediment properties: this is discussed further below.

[14] The nondimensionalized fluid continuity equation has the form

$$\frac{\partial h}{\partial t} + \frac{\partial}{\partial x}(Uh) = 0, \tag{1}$$

and it is usual to complete the description of the hydrodynamics with a horizontal momentum equation, typically including a quadratic drag law,

$$\frac{\partial U}{\partial t} + U\frac{\partial U}{\partial x} = -\frac{1}{F^2}\frac{\partial}{\partial x}(h - d) - K\frac{|U|U}{h}, \tag{2}$$

[see, e.g., *Friedrichs et al.*, 1998; *Roberts et al.*, 2000; *Pritchard et al.*, 2002], where the scaled drag coefficient $K \equiv c_D\hat{U}_0\hat{T}/\hat{\eta}_0$ is typically of order 1.

[15] We will make a further slight simplification: the global Froude number $F \equiv \hat{U}_0/(g\hat{\eta}_0)^{1/2}$ in equation (2) is typically of order 1/30 for tidal flows across flats, and so we consider the hydrodynamics in the limit $F \to 0$. In this limit, the momentum equation reduces to $\partial(h - d)/\partial x = 0$; the continuity equation (1) can then be rearranged to give

$$U(x, t) = \frac{\mathrm{d}\eta}{\mathrm{d}t}\frac{x_{sh} - x}{h(x, t)} \tag{3}$$

for any given tidal elevation $\eta(t)$. This simplified description has been used previously for morphological modeling of coastal environments, for example by *Friedrichs and Aubrey* [1996] and by *Schuttelaars and de Swart* [1999]. It describes the flow well except in a small region close to the shoreline where frictional effects may produce a distinct slope in the sea surface. On a flat of constant gradient, this region scales as $x_{sh} - x = O(F^2Ku^2)$, which is sufficiently small to be negligible throughout most of the analysis presented here; on the convex upper flat considered in section 3.1.2, it may be more significant, but is neglected for simplicity.

[16] Sufficiently fine sediment is transported principally in suspension. The vertical concentration profile may be characterized by a Rouse number $B = \hat{w}_s/(\kappa\hat{u}_*)$, where $\hat{w}_s$ is a particle settling velocity, $\hat{u}_*$ is a friction velocity and $\kappa \approx 0.4$ is the von Kármán constant. For flows over mudflats, typically $\hat{w}_s \approx 10^{-3}$ ms^{-1} and $\hat{u}_* \approx 2 \times 10^{-2}$ ms^{-1}, and so $B \approx 0.1$: we approximate further by assuming that sediment is well mixed in the water column. The ratio of the advective to the diffusive horizontal transport of suspended sediment, however, scales as $\hat{L}_x/\hat{L}_z$ and so is typically much greater than unity; throughout this study we therefore treat horizontal sediment transport as purely advective.

[17] Despite considerable experimental and field investigation, there are as yet no universally accepted models for the erosion and deposition of cohesive sediment. The most successful simple descriptions are those obtained experimentally, for deposition by *Einstein and Krone* [1962], and for erosion by *Partheniades* [1965]: these are common choices in mathematical and numerical modeling of estuarine sediment transport [see, e.g., *Dyer*, 1986; *Cancino and Neves*, 1999; *Brenon and Le Hir*, 1999]. The success of these studies, as well as the reasonable agreement with observational data [*Sanford and Maa*, 2001], suggests that these models capture the dominant sedimentary processes.

[18] We employ Partheniades' erosion model in its usual form, taking the mass erosion rate $\hat{Q}_e = \hat{m}_e(\hat{\tau}/\hat{\tau}_e - 1)$, where $\hat{\tau}$ is the bed shear stress, $\hat{\tau}_e$ is a critical stress which must be exceeded in order to break up the bed and entrain flocs, and $\hat{m}_e$ is a dimensional parameter. However, we employ a modified version of the Einstein-Krone deposition model.

[19] In the usual formulation, the mass deposition rate $\hat{Q}_d$ is the product of the suspended sediment concentration, the settling velocity $\hat{w}_s$ of a mud floc, and the probability p of a settling floc surviving the turbulence near the bed. The latter quantity is given by $p = 1 - \hat{\tau}/\hat{\tau}_d$, where $\hat{\tau}_d$ is a critical shear stress above which flocs break up and no longer settle. An undesirable feature of this model is that it provides no upper bound on the concentration of suspended sediment: in particular, SSC typically becomes unbounded at the shoreline, because there is no mechanism to counter the very rapid entrainment of flocs in shallow water.

[20] In field observations, a pronounced maximum of suspended sediment concentration, known as the "turbid tidal edge" (TTE), is often apparent at the start and end of inundation [*Christie and Dyer*, 1998]. High values of $\hat{C}$ may therefore be expected in this region, although the unboundedness of the concentration field is unphysical. In order to control this feature, the depositional model we consider includes the settling of suspended matter both in flocs and in the much smaller primary particles of which the flocs are built. The population of primary particles near to the bed is then given by $\hat{C}(1\text{-}p)$, and these particles settle at a rate $\hat{w}_p$, which is very much smaller than the floc settling velocity $\hat{w}_s$. The ratio $\epsilon = \hat{w}_p/\hat{w}_s$ is a complicated function of the sediment properties [*Winterwerp*, 2002]; we will treat it as a heuristic parameter, and demonstrate that our results are qualitatively unaffected by the value of the ratio ϵ, even in the limit $\epsilon = 0$, in which the Einstein-Krone formula is recovered.

[21] The parameters involved in the sediment transport equation provide natural scales for the cross-shore velocities and for sediment concentration. In order for both erosional and depositional processes to be nonnegligible, the reference cross-shore velocity $\hat{U}_0$ must be of similar magnitude to $\hat{U}_e$, the threshold velocity for sediment erosion; we shall see in section 4 how this estimate can be refined. We define a concentration scale which reflects a balance between erosive and depositional fluxes, $\hat{C}_0 = \hat{m}_e/\hat{w}_s$, so the sediment transport equation is given in nondimensional form by

$$\frac{\partial C}{\partial t} + U\frac{\partial C}{\partial x} = \frac{E}{h}[Q_e(U) - Q_d(U, C)], \quad \text{where} \tag{4}$$

$$Q_e = \begin{cases} \left(\dfrac{U^2}{U_e^2} - 1\right) & \text{for } |U| \geq U_e \\ 0 & \text{for } |U| < U_e \end{cases} \tag{5}$$

$$\text{and} \quad Q_d = \begin{cases} C\left(1 - (1-\epsilon)\dfrac{U^2}{U_d^2}\right) & \text{for } |U| \leq U_d \\ \epsilon C & \text{for } |U| > U_d. \end{cases} \tag{6}$$

The parameters U_e and U_d are the dimensionless threshold velocities for erosion and deposition respectively, and $E \equiv \hat{T}\hat{w}_s/\hat{\eta}_0$ is the dimensionless bed exchange rate, which is typically of order 1. It is generally found that $U_e > U_d$, and so periods of floc erosion and floc deposition are distinct: however, this has been questioned, and determining the critical stresses τ_e and τ_d remains a difficult experimental task [*Sanford and Halka*, 1993; *Sanford and Maa*, 2001]. We return to this point in Appendix C.

[22] The numerical studies of *Pritchard et al.* [2002] and *Roberts et al.* [2000] both impose a constant concentration, $C = C_{bdy}$, at the seaward boundary during the flood tide. This represents a uniformly turbid estuarine environment some distance offshore from the flat: it is a considerable simplification of the real system, in which the sediment input is controlled by longshore currents and offshore mixing processes, and is time dependent. In section 3 we will consider a more natural boundary condition.

[23] The morphodynamical equations may be completed by a bed evolution equation which gradually updates the bathymetry according to the net erosion or deposition at each point. Further details and discussion of this component are given by *Pritchard* [2001]; we need note only that under

normal circumstances, the bathymetry may be treated as static over tidal timescales.

2.2. Equilibrium States

[24] In this paper, we are not concerned with the general concept of equilibrium in coastal environments [*Kraus*, 2001]: it is sufficient to define the equilibrium state of a mudflat as that toward which it evolves under constant forcing conditions. The observations collated by *Kirby* [2000] suggest that a typical equilibrium state may be characterized by a constant cross-shore profile, measured relative to high water (HW) and low water (LW), which over decades migrates seaward or landward as sediment is imported to or exported from the system. We aim to characterize such an equilibrium profile.

[25] We define the net flux over a period,

$$Q(x; d(x)) \equiv \int_0^T q(x, t; d)\mathrm{d}t, \tag{7}$$

where in our shallow-water model the depth-integrated sediment flux $q(x, t)$ may be expressed simply as $q = CUh$, and where the hydrodynamic variables $h(x, t)$ and $U(x, t)$, and the suspended sediment concentration $C(x, t)$, vary with period T. The residual fluxes associated with advance or retreat which take place over tens of thousands of tides must be very much smaller than the instantaneous flux of sediment across the flat, and so an equilibrium profile $d(x) = d_{\mathrm{eq}}(x)$ must approximately satisfy the condition $\mathrm{d}Q/dx = 0$ at every position x across the flat. In section 3, we will develop periodic solutions for $C(x, t)$, and then investigate the quantity $Q(x)$ which determines the morphodynamics of the flat.

[26] In recent years, a number of comprehensive studies [*Kirby*, 1992; *Dyer*, 1998; *Kirby*, 2000] have established a basic typology of mudflat morphology. For tidally dominated flats, the canonical morphology is convex: the gradient is approximately constant across the lower part of the flat and reduces to almost zero at the high-water mark.

[27] The first explanation of this morphology was provided by *Friedrichs and Aubrey* [1996]. They assumed that the peak shear stress (and thus the peak velocity) during a tidal cycle was uniform across an equilibrium tidally dominated flat. Assuming equation (3), and taking a sinusoidal tidal elevation curve, it is straightforward to derive the profile

$$\hat{d}_{\mathrm{eq}}(\hat{x}) = \begin{cases} -\frac{1}{2}\hat{\eta}_0 \dfrac{\hat{x}}{\hat{L}_0} & \text{for } \hat{x} \le 0 \\ -\frac{1}{2}\hat{\eta}_0 \sin\left(\dfrac{\hat{x}}{\hat{L}_0}\right) & \text{for } \hat{x} \ge 0. \end{cases} \tag{8}$$

Here mean sea level (MSL) occurs at $\hat{x} = 0$, and we define $\hat{L}_0 = \hat{U}_0\hat{T}/2\pi$, where $\hat{U}_0$ the maximum velocity reached during the tidal cycle. We shall refer to this profile as an FA96 flat.

[28] Equation (8) provides a good qualitative model for the tidally dominated flats described by *Kirby* [2000] and by *Friedrichs and Aubrey* [1996], and we will employ it as a prototypical description of an equilibrium, linear-convex flat (see section 3.1.2). However, as muddy sediments are easily transported long distances in suspension [*Lee and Mehta*, 1997], the use of a local dynamical balance to describe global equilibrium requires some justification: this will be discussed in section 3.2.3.

[29] Numerical studies of mudflat evolution have been carried out by *Roberts et al.* [2000], by *Pritchard et al.* [2002], and recently also by B. Waeles et al. (Modélisation morphodynamique cross-shore d'un estran vaseux, submitted to *Compte Rendus Geoscience*, 2002, hereinafter referred to as Waeles et al., submitted reference, 2002). The models employed varied in complexity, although they shared the main features of that described in the current study, and the overall character of their results was very similar. Typical equilibrium profiles were approximately linear below mean sea level and convex above, and the peak velocity $\hat{U}_{\max}$ was approximately constant across the flat (except on the upper part of *Roberts et al.*'s [2000] flats, where the model became dynamically inconsistent). In the models of both *Pritchard et al.* [2002] and Waeles et al. (submitted reference, 2002), the equilibrium profile became established over a few decades, and the flat then migrated seaward while maintaining a constant profile, in agreement with Kirby's findings. Both *Roberts et al.* [2000] and *Pritchard et al.* [2002] found that the mean gradient of their flats increased in proportion to the tidal range, and decreased with greater sediment supply: we discuss these trends in section 4.

3. Sediment Transport Under Tidal Currents

[30] We will now construct solutions for suspended sediment concentration within the model outlined above. This reduced model retains much of the dynamical complexity which is observed in the field and in more complicated simulations: our solutions therefore provide a "laboratory" in which we can investigate the processes which lead to net sediment transport. This allows us to elucidate the classical descriptions of settling lag [*van Straaten and Kuenen*, 1958; *Postma*, 1961] as an agent of net sediment transport, and provides insight into the subtleties of this mechanism.

[31] The other important result which these solutions provide is a physical relationship between the gradient of a flat and the offshore SSC, which represents the sediment supply to the morphodynamical system. This result will be used in section 4 to obtain estimates for the equilibrium gradient of flats under given external conditions.

[32] We first consider a flat with a linear cross-shore profile (section 3.1.1), which has the advantage that we may construct exact analytical solutions; we then consider a more realistic linear-convex geometry (section 3.1.2).

3.1. Constructing Solutions in a Lagrangian Frame

[33] While it is necessary to work in an Eulerian frame in order to describe the evolution of the bed, it is more natural to consider the short-term dynamics in a Lagrangian frame. In such a description, we consider fluid elements with position $x_{\mathrm{L}}(t; x_0)$ such that $x_{\mathrm{L}}(0, x_0) = x_0$, depth $h_{\mathrm{L}}(t; x_0)$ and velocity $U_{\mathrm{L}}(t; x_0)$, and carrying sediment concentration $C_{\mathrm{L}}(t; x_0)$. The sediment transport equation (4) can now be written as a pair of ordinary differential equations,

$$\frac{\mathrm{d}C_{\mathrm{L}}}{\mathrm{d}t} = \frac{E}{h_{\mathrm{L}}}[Q_e(U_{\mathrm{L}}, t) - Q_d(U_{\mathrm{L}}, C_{\mathrm{L}}, t)] \quad \text{on trajectories } \frac{\mathrm{d}x_{\mathrm{L}}}{\mathrm{d}t} = U_{\mathrm{L}}(t), \tag{9}$$

which may be integrated analytically or numerically. Appendix A describes how periodic solutions may be

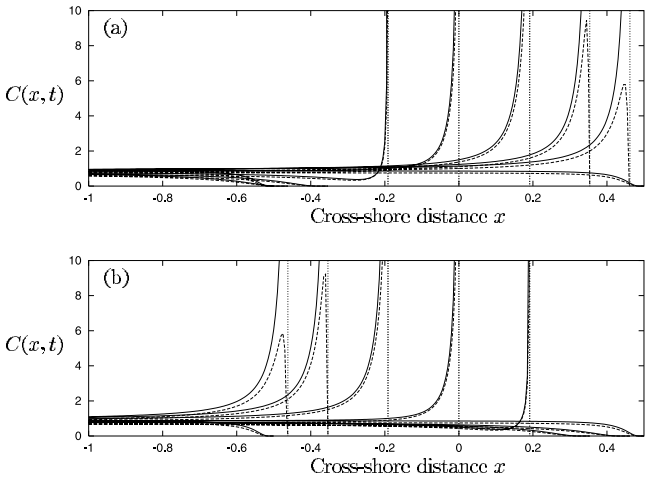

Figure 2. Analytical solution for SSC on a linear flat, with $U_e = 0.8$ and $U_d = 0.4$: (a) flood and (b) ebb. Plots are at intervals of $\pi/16$. Solid lines represent $\epsilon = 0$; dashed lines represent $\epsilon = 0.025$. The vertical axis is cut off at $C = 10$ for visual convenience.

constructed for the Lagrangian quantity C_L, and thus for the Eulerian suspended sediment concentration: we now discuss these solutions for two particular bathymetries.

3.1.1. Sediment Transport Across a Linear Flat

[34] On a flat of constant gradient, $d(x) = -x$, and under a sinusoidal tide, we may obtain an exact analytical solution for the SSC, following the method outlined in Appendix A.

[35] The Eulerian solutions for two values of ϵ are plotted, at intervals of 1/16 of a tidal period, in Figure 2. These plots show the gradual entrainment of sediment and the formation of the turbid tidal edge during the period when $U > U_e$, as well as the very rapid collapse of the TTE when U falls below U_d.

[36] During erosional periods, the concentration for $\epsilon = 0$ becomes unbounded at the shoreline. In contrast, the particulate settling term ϵC imposes a finite concentration $C_{eq} = \epsilon^{-1}(U^2/U^2_e - 1)$ at the shoreline during erosional phases, and causes the concentration to drop to zero during purely depositional phases. However, this corresponds to only a small change in the actual quantity of sediment in suspension, which is given by Ch, and this is reflected in the small change which occurs in the cross-shore sediment fluxes discussed in section 3.2.2. (The effect of further altering the erosional and depositional fluxes is considered in Appendix B.)

[37] Another important feature of this solution is that the concentration of suspended sediment tends to a constant value at large distances from the shoreline, $C(x, t) \to C_\infty$ as $x \to -\infty$, where C_∞ is a function of U_e, U_d and ϵ. This deep-water value can be obtained most easily by employing the conservation of sediment in deep water: since the total deposition from a fluid element over a cycle must equal the total erosion over that cycle, we must have

$$\lim_{|x_0|\to\infty} \int_0^T Q_e(U_L(t); x_0)\mathrm{d}t = \lim_{|x_0|\to\infty} \int_0^T Q_d(C_\infty, U_L(t); x_0)\mathrm{d}t, \tag{10}$$

leading to

$$C_\infty = \frac{U_d^2}{U_e^2} \cdot \left[\frac{U_e\sqrt{1-U_e^2} + \left(1-2U_e^2\right)\cos^{-1} U_e}{(1-\epsilon)\left[U_d\sqrt{1-U_d^2} + \left(2U_d^2-1\right)\sin^{-1} U_d\right] + \epsilon U_d^2 \pi} \right]. \tag{11}$$

[38] The limiting offshore concentration C_∞ given by equation (11) is important because it sets the scale for the sediment dynamics of the system: if processes in the more landward parts of the flat lead to local levels of suspended sediment which are very much lower or higher than this, then the resulting cross-shore gradient of SSC will mean that advective transport imports or exports large quantities of sediment, changing the morphology and thus the local dynamics. As we will show in section 4, this allows us to use equation (11) to relate the gradient of the flats to the supply of sediment from the offshore region.

[39] In Figure 3, the residual flux Q is plotted at various points across the flat. Particularly in the intertidal region, there is a clear landward movement of sediment, which decays rapidly to zero below LW (though it is not quite symmetrical across the intertidal region, and there is some small flux as far seaward as about $x = -0.6$). The effect of this flux is to move sediment from the lower to the upper flat: there is no import of sediment from far offshore (the limit $x \to -\infty$). We discuss this further in section 3.2.2.

3.1.2. Sediment Transport Across a Linear-Convex Flat

[40] We now consider the suspended sediment transport on a flat of the type described by equation (8). An analytical solution is not available, but given the velocity field provided by equation (3), periodic solutions may be obtained numerically as described in Appendix A. The flat considered here has the critical velocity $U_0 = 1$, and the sediment parameters are the same as for the analytical solution plotted in Figure 2: $E = 1$, $U_e = 0.8$ and $U_d = 0.4$.

[41] Figure 4 shows snapshots of the periodic concentration field at intervals of 1/16 of a tidal period. There are some obvious similarities to the exact solution on a linear flat (Figure 2). In particular, toward the seaward end of the domain, the concentration field $C(x, t)$ is very similar to that

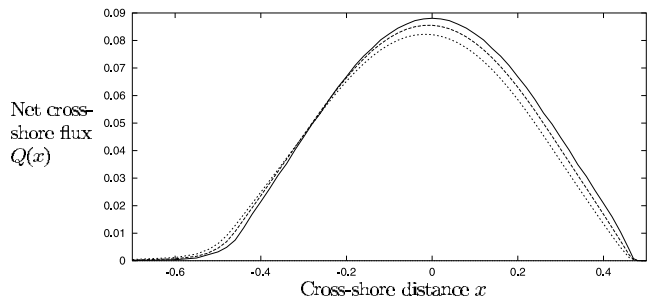

Figure 3. Residual landward sediment flux $Q(x)$ across a linear flat, for $\epsilon = 0$ (solid line); $\epsilon = 0.01$ (dashed line); and $\epsilon = 0.025$ (dotted line). (Note MSL is at $x = 0$; HW and LW are at $x = \pm 0.5$.)

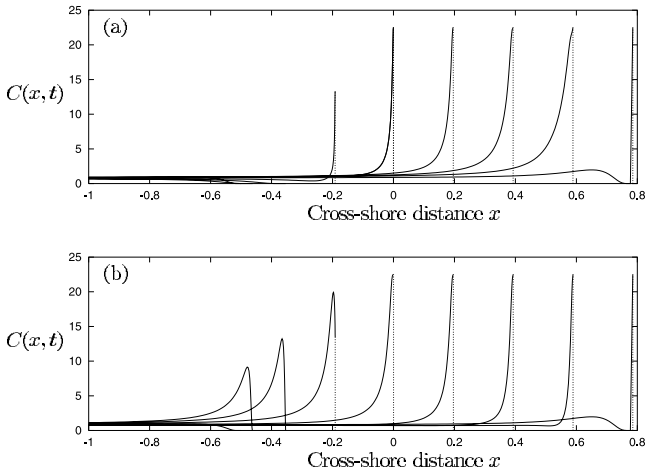

Figure 4. Numerical results for SSC on an FA96-type flat (MSL at $x = 0$), with $U_e = 0.8$, $U_d = 0.4$, $\epsilon = 0.025$: (a) flood and (b) ebb. Plots are at intervals of $\pi/16$.

on the linear flat. In fact, the deep-water concentration C_∞ defined by equation (11) also provides the limiting value of $C(x, t)$ in this case, and the convergence of C to C_∞ is rather rapid as $|x|$ increases.

[42] The major difference between the linear and the linear-convex flat is the behaviour of the turbid tidal edge. On the upper flat, the decreasing gradient, and consequently higher velocities, maintain the TTE throughout the flood, and allow it to form again rapidly on the ebb. (The reduced settling at high-water slack means that concentrations generally are noticeably higher than on the linear flat, although the overall dynamics are very similar.) A peculiar feature is that the TTE at the shoreline never collapses, since the shoreline is accelerated instantaneously from $U = 1$ to $U = -1$ at high-water slack. This is an artifact of the idealized bathymetry and the inertialess hydrodynamic model, and does not affect the sediment budget across the flat.

[43] Figure 5 shows the net cross-shore flux $Q(x)$ over a tidal cycle. Perhaps surprisingly, the net flux resembles the linear case most on the upper flat, where there is a small net landward movement of sediment. On the lower part of the flat and in the subtidal region, though, the net flux is seaward, and the decay of $Q(x)$ is much more gradual than on the linear flat. This is discussed further in section 3.2.3.

3.2. Interpretation and Discussion of Solutions

[44] The processes leading to net sediment transport may be interpreted either in Lagrangian form, in terms of the processes known as settling lag and scour lag, or in Eulerian form, by considering the cross-shore fluxes of suspended sediment $q(x, t)$ and $Q(x)$. The standard conceptual descriptions of sediment transport [see, e.g., *Nichols and Biggs*, 1985] are essentially Lagrangian, whereas recent field studies of intertidal flats [e.g., *Christie et al.*, 1999; *Bassoullet et al.*, 2000] have sought to describe the Eulerian sediment fluxes. The form of our solutions makes it natural to compare these two interpretations, in order to establish what are the observable "signatures" of lag effects, how they operate in different parts of the system, and when this concept may be usefully applied.

3.2.1. Settling and Scour Lag Effects

[45] The processes of settling lag and scour lag were proposed by *van Straaten and Kuenen* [1958] and by *Postma* [1961] to explain the accumulation of fine sediment in the landward reaches of tidal inlets. The basic mechanism of settling lag is that a suspended sedimentary particle takes a finite time to settle out of suspension, and thus is carried landward on the flood some distance after the local fluid velocity has fallen below the threshold for deposition. It is therefore reentrained on the ebb not into the fluid element which deposited it, but into one located further landward. (This process is accentuated, "scour lag", if the threshold velocity for the erosion of sediment is higher than the threshold velocity for deposition: for simplicity, we neglect scour lag in this discussion.) Figure 6 illustrates the settling lag process in schematic form [cf. *van Straaten and Kuenen*, 1958, Figure 2].

[46] When the hydrodynamics are spatially uniform (Figure 6a), no net transport can occur. A particle is entrained on the flood tide (A) and carried until just before HW slack (HWS), when the current drops below the threshold for deposition; it settles gradually, reaching the bed (B) a distance Δ_{HW} beyond the point at which it started settling. On the ebb, the particle is reentrained by a more landward fluid element, which carries it seaward until it starts to sink shortly before LW slack (LWS); finally, it is deposited again (C) a distance Δ_{LW} beyond where it started to sink. Since the trajectories of all fluid elements are identical and the settling distances Δ_{HW} and Δ_{LW} are the same, the particle is redeposited where it started off.

[47] If fluid velocities are uniform but depths are not, the settling distance at HWS may exceed that at LWS (Figure 6b). In this case, the particle is deposited further landward than it started; similarly, if $\Delta_{HW} < \Delta_{LW}$ we may expect net seaward transport. Conversely, Figure 6c shows a case where the settling distances are identical, but the fluid trajectories are not. Here, the smaller excursion of the more landward fluid element means that the particle is deposited further landward than it started; similarly, if the tidal excursion increased landward, the particle would be deposited further seaward than it started.

[48] Although this mechanism is generally described in terms of individual sedimentary particles, it can be applied to a model of the type described in this paper, where a continuous sediment concentration $C(x, t)$ is employed to represent the stochastic nature of sediment response. In a continuum description, the particulate settling time is

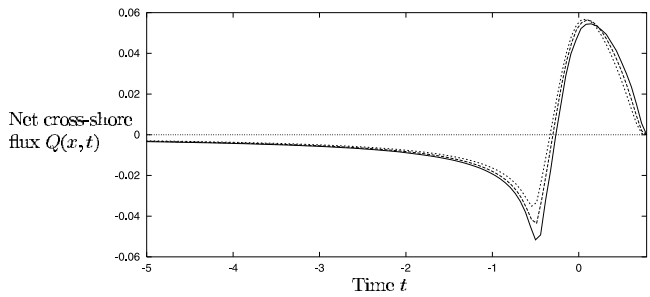

Figure 5. Net cross-shore flux $Q(x)$ on an FA96-type flat, with $U_e = 0.8$, $U_d = 0.4$, $E = 1$, and $\epsilon = 0$ (solid line); $\epsilon = 0.01$ (dashed line); and $\epsilon = 0.025$ (dotted line).

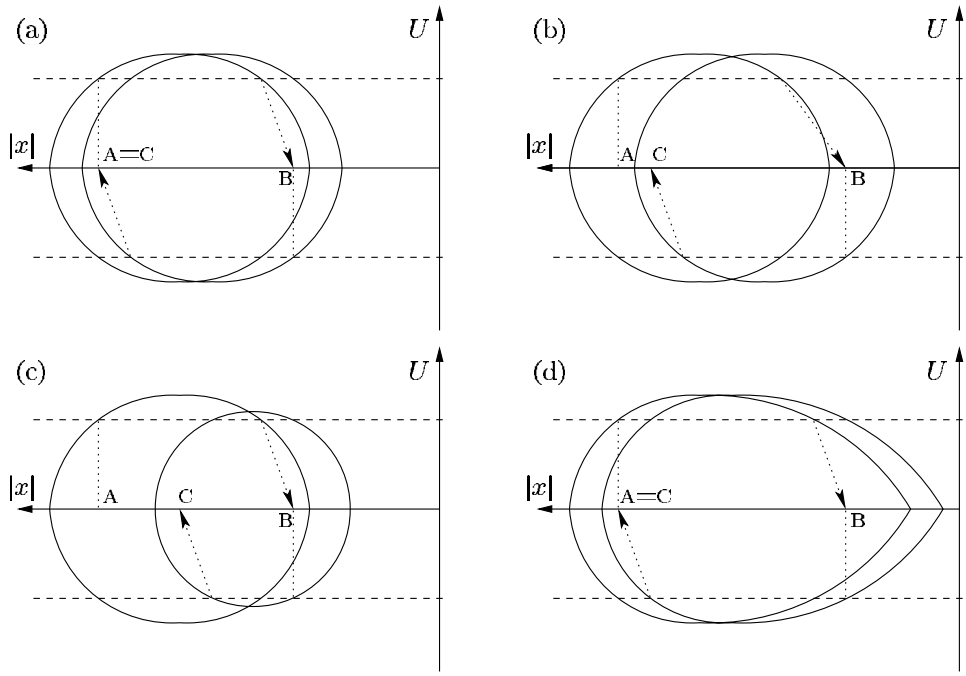

Figure 6. Schematic illustration of some mechanisms of settling lag. Solid lines indicate trajectories of fluid elements; dashed lines indicate $U = \pm U_d$; and dotted lines represent particle settling and reentrainment. (See text for discussion.)

generalized to the time taken for the concentration field to respond to changes in the fluid velocity, which is quantified in our model by the dimensionless exchange rate E. We will discuss the limits of this interpretation below.

[49] In tidal inlets, the maximum velocity and tidal excursion of a fluid element increase seaward, so the mechanism illustrated in Figure 6c may lead to net landward transport [*van Straaten and Kuenen*, 1958]. *Postma* [1961] proposed an alternative mechanism, which depends on hydrodynamic asymmetries. The length of HWS typically exceeds that of LWS, leading to greater total deposition, and thus to lower concentrations on the ebb than on the flood: this was later demonstrated in a mathematical model by *Groen* [1967]. As Figure 6d illustrates, this is not predicted by a particulate model of sediment dynamics, because the settling distance of an individual particle does not depend on the length of slack water. It is generally believed [see, e.g., *Nichols and Biggs*, 1985] that in many estuarine contexts these two mechanisms work together to promote the landward movement of sediment.

3.2.2. Transport Patterns Across a Linear Flat

[50] In tidal flow over a linear flat, the distance-velocity trajectories and the durations of HWS and LWS are identical for all fluid elements. However, the element which carries a particle on the ebb tide is located further landward than that which carries it on the flood tide. Hence the fluid depth h_L is smaller, the particle takes less time to settle out around LWS, and $\Delta_{LW} < \Delta_{HW}$, leading to net landward transport.

[51] The instantaneous sediment fluxes $q(x, t)$ at several points across the flat are shown in Figure 7. We recall that in the Lagrangian frame, concentration varies with twice the frequency of the fluid motion, and so the lag of SSC behind velocity must be identical on the flood and on the ebb. However, in the Eulerian frame, because the sediment-laden region is advected backward and forward the phase relation is correspondingly advanced or retarded, and so the fluxes become asymmetrical and do not cancel out when integrated over a tidal cycle.

[52] Even at points below LW (such as $x = -1$) where there is a net balance between seaward and landward fluxes, the sediment fluxes are different on the flood and on the ebb. The peak flux on the flood is higher, but because it occurs when the fluid velocity is already falling and as lower concentrations are being advected landward from the offshore region, it is shorter lived; whereas the peak on the ebb occurs slightly before maximum ebb velocity, and so although it is lower, it is sustained for longer by the entrainment of sediment and by the seaward advection of the high concentrations associated with the turbid tidal edge. In the intertidal region, the sediment flux lags still further

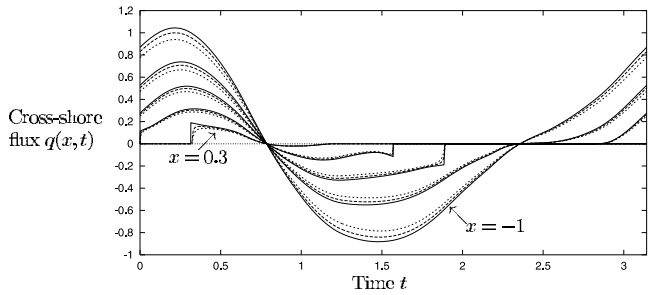

Figure 7. Landward sediment flux $q(x, t)$ as a function of time, for $x = -1$, -0.6, -0.3, 0, and 0.3. Physical parameters and legend are as in Figure 3. Note that q is typically 10 times larger than the net flux Q, even over this highly nonequilibrium bathymetry.

behind the fluid velocity, and this is particularly noticeable on the upper flat on the ebb (compare the times at which the local minimum of q occurs for the values of x plotted in Figure 7).

[53] The phase lag between velocity and sediment concentration is the Eulerian "signature" of the settling lag process described above. It occurs essentially because the dynamics of suspended matter are naturally Lagrangian in character, while sediment exchanges with the bed must be considered in an Eulerian frame. When a particle is deposited and reentrained, the lag effect means that it changes its position in the Lagrangian but not in the Eulerian frame; correspondingly, a phase lag in the Eulerian frame corresponds to the transfer of material between fluid elements in the Lagrangian frame.

[54] Finally, we note that, as indicated in section 3.1.1, the particulate settling term proportional to ϵ does not alter the qualitative character of the results. The effect of this term is evident in the plots of q (Figure 7) near the start and end of inundation, where it causes the flux to drop off more rapidly, and it is also evident in figure 3 that increasing ϵ leads to slightly greater net sediment movement below low water. This is discussed further in Appendix B.

3.2.3. Transport Patterns Across a Linear-Convex Flat

[55] In tidal flow over a linear-convex flat, the transport mechanisms become more complicated. The convexity causes tidal excursion to increase landward, promoting the export of sediment (Figure 6c). Fluid depths are generally lower around HWS, and the higher velocities on the upper flat reduce the duration of HWS, decreasing Δ_{HW} relative to Δ_{LW}, which should accentuate this effect.

[56] To explain the net landward transport seen on the upper flat (Figure 5), we require a continuum description of the dynamics. Because of the smaller depths, much more sediment is able to deposit at HWS than at LWS, leading to lower concentrations during the ebb than during the flood, and thus to a net landward flux of sediment. (A similar process was suggested by the observations of *Wang and Eisma* [1990], although in that case landward transport was considerably enhanced by the asymmetry of the tidal curve.) This effect is most significant in shallow water, where the proportional difference in fluid depth is greatest. Consequently, this mechanism dominates on the upper flat; further seaward, lag effects associated with the difference in excursion start to dominate, and we see a small net seaward flux.

[57] Far from the shore, the particulate interpretation again becomes misleading, because the water is sufficiently deep that typical settling times are comparable to the period of the fluid motion. The seaward transport here can best be explained by considering the behaviour of a fluid element far from the shore. The basic variation of concentration here has twice the frequency of the tide. However, the presence of the convex upper flat enhances velocities while it is inundated, thus suppressing deposition around HWS, and enhancing erosion during the end of the flood and the start of the ebb phases. The net result is that sediment concentrations are slightly higher on the ebb than on the flood, leading to a net seaward flux of suspended sediment. This illustrates the sensitivity of net sediment transport to the presence of gently sloping flats close to high water remarked on by *Dronkers* [1986].

3.2.4. Conclusions: Settling Lag on Intertidal Flats

[58] These results illustrate how the finite settling time of a sedimentary particle translates into a phase lag between velocity and suspended sediment concentration in an Eulerian frame. Settling lag does not depend on asymmetries in the distance-velocity curve of a fluid element, although it may be affected by them. Unlike the spatial nonuniformities introduced by friction and bathymetry in shallow inlets, those introduced by the bathymetry of a convex flat may either enhance or reduce net transport, and settling lag may play different roles in different regions of the tidal system. To explain these effects, a continuum rather than a particulate model of sediment dynamics is required in regions where settling times exceed the period of the fluid motion, or where (as on the upper part of a convex flat) a large proportion of the sediment in suspension is able to settle out in a short time.

[59] Without the assistance of asymmetry in the distance-velocity curve the net landward transport induced by settling lag may be confined to a rather small region mostly situated above the low-water mark (Figure 3). The role of settling lag under these circumstances is to supply the upper flat with material drawn mainly from the lower flat, but not to import sediment from regions further offshore. Figure 5 illustrates the more unexpected result that under some circumstances, settling lag can lead to a net seaward movement of sediment in the region further from the shore. As most treatments of settling lag focus on its potential for purely landward transport, this possibility merits further attention. In particular, it would be interesting to determine whether seaward transport offshore from convex flats can be identified in the field.

[60] The different patterns of net transport on the identical subtidal parts of the linear and linear convex flats illustrate the nonlocal dynamics which make it hard to characterize an equilibrium bathymetry. Despite this, the Friedrichs-Aubrey criterion provides a reasonable approximation to equilibrium. This is not, as *Friedrichs and Aubrey* [1996] suggested, because uniform peak velocities across the flat lead to zero divergence in the net sediment transport: although the peak velocities are dynamically the most important, settling lag effects depend on the shape as well as the magnitude of the fluid velocity-distance trajectories. The criterion does impose some uniformity on these trajectories; more importantly, it defines a bathymetry in which the lag effects due to nonuniformities in the tidal excursion compete with, and partially cancel out, those due to variations in the fluid depth. Consequently, equation (8) provides a good working approximation to an equilibrium flat.

4. Characterizing Equilibrium Morphologies

[61] So far, we have considered the short-term processes of sediment transport, taking the bathymetry of the flat, and its overall dimensions, as given. However, in a natural tidal setting which exhibits morphodynamic equilibrium, there must be some relationship between the large-scale morphology and the sediment properties and supply: knowing this relationship, we should be able to construct a priori estimates for the morphology which will develop under given conditions. We now consider this relationship in more detail.

[62] Motivated by the results of section 3.2.3 and by the studies summarized in section 2.2, we will assume that the equilibrium profile of a flat becomes linear far from the shore. This has two consequences. First, the morphology may be characterized by the single quantity $\hat{U}_0$: we recall from section 2 that the vertical length scale of the flat is defined by the tidal range $\hat{\eta}_0$, while the horizontal length scale is given by $\hat{L}_x = \hat{U}_0\hat{T}$; thus the gradient scales with $\hat{L}_z/\hat{L}_x = \hat{\eta}_0/(\hat{U}_0\hat{T})$. For a given linear or linear-convex flat, we may choose $\hat{T}$ and $\hat{U}_0$ (as in section 3) so that $\hat{U}_0$ is the maximum velocity $\hat{U}_{\max}$ attained under a sinusoidal tide, and $\hat{\eta}_0/(\hat{U}_0\hat{T})$ defines the gradient of the flat.

[63] Second, the equation (11) describes the relationship between the sediment properties and the offshore levels of suspended sediment. This then provides a connection between the sediment properties and supply and the gradient of the flats, since this gradient enters through the definition of the dimensionless threshold velocities for erosion and deposition, $U_e = \hat{U}_e/\hat{U}_0$ and $\hat{U}_d = \hat{U}_d/\hat{U}_0$. Given the physical parameters $\hat{U}_e$, $\hat{U}_d$, $\hat{m}_e$, and $\hat{w}_s$, and an offshore concentration $\hat{C}_\infty$, we may then invert equation (11) to obtain $\hat{U}_0$, and thus the gradient of a corresponding linear flat.

[64] We may relate this process to the numerical experiments of *Roberts et al.* [2000] and *Pritchard et al.* [2002] if we identify the imposed boundary concentration $\hat{C}_{\text{bdy}}$ with the deep-water limit $\hat{C}_\infty$, and nondimensionalize so that the resulting value of $\hat{U}_0$ represents the maximum velocity on the linear part of the flat. We expect that a flat will adjust from a given initial condition until this condition is satisfied, and there is no longer a tendency to import or export sediment from far offshore.

4.1. Equilibrium Flats Under a Sinusoidal Tide

[65] We first consider a sinusoidal tide, as in section 3. In Figure 8, we assume that the ratio $\hat{U}_e/\hat{U}_d$ is fixed, and show the variation of $1/\hat{U}_e \equiv \hat{U}_0/\hat{U}_e$ with C_∞. (We recall that the gradient scales as $\hat{U}_0^{-1}$, so higher velocities correspond to a more gently sloping flat.) As C_∞ increases, so does $\hat{U}_0$: the physical reason for this is that higher velocities are required to maintain the higher quantities of sediment in suspension. The value of ϵ slightly alters the estimate for $\hat{U}_0$, since higher values of ϵ increase the net deposition rate, and so require slightly higher velocities in order to balance this.

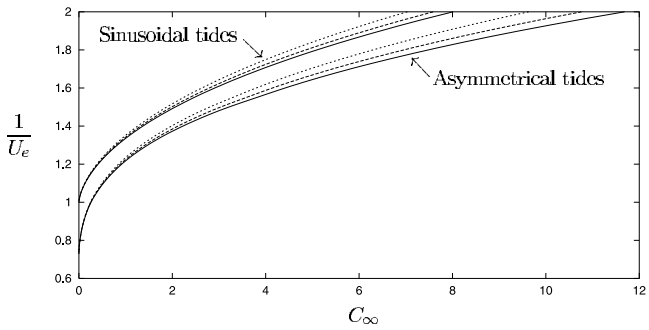

Figure 8. The quantity $1/U_e$, which is proportional to the dimensional velocity $\hat{U}_0$, plotted as a function of the dimensionless deep-water concentration C_∞, for $U_e = \sqrt{2}U_d$, under symmetrical tides (section 3.1.1) and asymmetrical tides (section 4.2.1): $\epsilon = 0$ (solid lines); $\epsilon = 0.01$ (dashed lines); and $\epsilon = 0.025$ (dotted lines).

Table 1. Dependence of Critical Velocity and Flats Gradient on $\hat{C}_{\text{bdy}}$: Theoretical Predictions $\hat{U}_0$ (Velocity) and S_0 (Gradient) Compared With Values $\hat{U}_{\max}$ and S_{lin} Estimated From the Data of *Roberts et al.* [2000][a]

	Theoretical		Numerical		
$\hat{C}_{\text{bdy}}$, kg m^{-3}	$\hat{U}_0$, ms^{-1}	S_0	$\hat{U}_{\max}$, ms^{-1}	S_{lin}	Relative Error
0.025	0.363	0.00160	0.373	0.00156	2.7%
0.1	0.422	0.00138	0.416	0.00140	1.4%
0.2	0.472	0.00123	0.489	0.00119	3.5%
0.4	0.534	0.00109	0.534	0.00109	0.0%

[a]Relative errors are given by $(\hat{U}_0 - \hat{U}_{\max})/\hat{U}_0$.

[66] To test our basic assumption that a flat will adjust until $C_{\text{bdy}} = C_\infty$, we compare our estimates for the peak velocity and for the gradient of the flat with the results of *Roberts et al.* [2000]: these were obtained using an identical dynamical model, with $\epsilon = 0$. Estimates of $\hat{U}_0$ can be obtained from *Roberts et al.*'s [2000] data by measuring the gradient of the near-linear lower part of each flat, and using equation (3).

[67] *Roberts et al.* [2000] found that flats with different tidal ranges had identical peak shear stresses on the lower flat: this agrees with our estimates, since the horizontal velocity $\hat{U}_0$ is set independently of $\hat{\eta}_0$. The variation of the gradient with $\hat{C}_{\text{bdy}}$ is also in excellent accordance with the estimates provided by equation (11). These estimates and numerical results are compared in Table 1. The agreement is within the margin of error both of the measured gradients of *Roberts et al.*'s [2000] flats and of our estimates, and suggests that in the dynamical regime of equation (3), our estimates capture the variation of the gross morphology.

[68] We can assess the effect of including a more complete hydrodynamical model by comparing our estimates with the calculations of *Pritchard et al.* [2002] for the case $\epsilon = 0$. Table 2 shows the peak velocities and approximate gradients for the various cases considered by *Pritchard et al.* [2002]. We show separately the numerical results for the subtidal region in which the flat is near linear, and the intertidal region in which the flat is convex.

[69] Our estimates describe the gross morphology of the subtidal region reasonably well, though they are poorer for higher boundary concentrations. The errors are generally of the order of a few percent, and so are comparable with the errors which we may expect to be introduced by identifying C_{bdy} (which is imposed at a finite distance from the shoreline) with C_∞ (which is the deep-water limit).

[70] The gross morphology of the intertidal region varies somewhat more weakly with $\hat{C}_{\text{bdy}}$ than our estimates

Table 2. Maximum Current Speeds $\hat{U}_{\max}$ for Equilibrium Flats, Compared With Theoretical Predictions for $\hat{U}_0$[a]

		Theoretical		Subtidal		Intertidal	
$\hat{\eta}_0$, m	$\hat{C}_{\text{bdy}}$, kg m^{-3}	$\hat{U}_0$, ms^{-1}	S_0	$\hat{U}_{\max}$, ms^{-1}	S_{sub}	$\hat{U}_{\max}$, ms^{-1}	S_{int}
8	0.025	0.223	0.00261	0.226	0.00257	0.226	0.00257
8	0.1	0.273	0.00213	0.262	0.00222	0.262	0.00222
8	0.2	0.305	0.00191	0.287	0.00203	0.268	0.00217
8	0.4	0.366	0.00159	0.329	0.00177	0.268	0.00217
6	0.1	0.273	0.00160	0.256	0.00170	0.238	0.00183
4	0.1	0.273	0.00107	0.256	0.00114	0.226	0.00129

[a]The numerical experiments employed $c_D = 0.006$, $\hat{w}_s = 1$ mm s^{-1}, $\hat{m}_e = 5 \times 10^{-5}$kg m^{-2} s^{-1}, $\hat{U}_e = 0.183$m s^{-1} and $\hat{U}_d = 0.129$m s^{-1}.

predict, with a maximum error of just over 25% for the case $C_{\mathrm{bdy}} = 0.4$ kg m^{-3}. This is not surprising, given that the theory is based around a deep-water approximation to the flow field which is least applicable near the shoreline. The discrepancy may be due to the more complicated dynamics represented in the numerical model: in particular, the effects of frictional drag can no longer be neglected and strongly influence the dynamics in very shallow water. It is also possible that, since SSC in the intertidal region varies considerably over a cycle, the influence of the offshore region is swamped by local processes. In this case, the coupling between the subtidal and intertidal morphology may be rather weak, and we might expect the numerical experiments to have difficulty resolving equilibrium states accurately.

[71] The overall agreement between analytical and numerical results suggests that equation (11) captures the essential relationship between equilibrium morphology and sediment supply. In Appendix C we consider the implications that this has for morphological modeling of systems in which some of the material properties, such as the erosion threshold $\hat{U}_e$, are not precisely known.

4.2. Extension to Other Tidal Signals

[72] While the analysis presented above is a useful starting point for understanding the morphology of tidally dominated flats, most muddy coasts experience a more complex tidal regime. The most significant longer-term variation in the tidal signal [see *Dyer*, 1986] is the spring neap cycle with an approximate period of two weeks. In the macrotidal environments typical of tidally dominated flats, the neap-spring variation in tidal range may be as large as several meters, with corresponding variations in the strength of the cross-shore currents. In addition, the tidal curve experienced by most mudflats is affected by the propagation of the tidal wave in the surrounding coastal region, and is generally not sinusoidal [*Le Hir et al.*, 2000]. We will therefore consider both asymmetrical tides and tides which experience a spring-neap cycle.

[73] Under these conditions, the scaling velocity $\hat{U}_0$ cannot necessarily be identified with the maximum current velocity $\hat{U}_{\max}$. However, the numerical results of *Pritchard et al.* [2002] suggest that both tidal regimes result in a convex flat which becomes approximately linear at large distances from the shoreline, and so $\hat{U}_0$ may still be used to characterize the gradient of this region, even if it is no longer identical to $\hat{U}_{\max}$.

[74] For anything other than a very simple form of $\eta(t)$, it is rather laborious to construct an exact solution for the Lagrangian concentration field $C_{\mathrm{L}}(t; x_0)$. However, we can make use of the facts that, on a linear flat, $U(x, t) = U(t)$, and $C(x, t)$ tends to a constant C_∞ far from the shore. We can then find C_∞ as the solution of equation (10), so that sediment conservation in a fluid element is satisfied in the deep-water limit, and thus determine how the tidal asymmetry affects the gross morphology. In general, $C_\infty(U_e, U_d)$ must be determined numerically, solving (10) by bisection or a similar method.

4.2.1. Ebb- and Flood-Dominated Tides

[75] For illustration, we consider the asymmetrical tides $\eta_{\pm}(t) = a\left[\cos 2t \pm \frac{1}{4}\sin 4t\right]$, where the constant $a = 0.454$ is chosen to give the tide a dimensionless range of 1. These correspond respectively to ebb- and flood-dominated regimes: in fact both tides give the same result for C_∞ because only $|U|$, rather than U, is significant when determining the deep-water concentration.

[76] In Figure 8, the corresponding $C_\infty(U_e, U_d)$ is compared to the result for the symmetrical tide. The most obvious difference is that, under the asymmetrical tide, the deep-water concentration reaches 0 only for $U_e = 3a = 1.36$ (corresponding to the maximum velocity reached during the cycle). This means that a state in which no sediment is eroded or deposited can occur only for a rather steeper flat, on which current speeds are lower. In general, any C_∞ requires a steeper flat under the asymmetrical than the symmetrical tide: for example, $C_\infty = 2$ requires $U_e = 0.67$ for the symmetrical and $U_e = 0.75$ for the asymmetrical tide. This is because the sediment dynamics are dominated by the higher velocities because of the nonlinear dependence of sediment transport on U.

[77] Numerical experiments carried out by *Pritchard et al.* [2002] using these tidal signals produced equilibrium flats which, under a symmetrical tide, experienced a maximum current speed of between 0.214 ms^{-1} (in the intertidal region) and 0.244 ms^{-1} (in the subtidal region). This compares well with the estimated value of 0.244 ms^{-1} which may be obtained from Figure 8 using *Pritchard et al.*'s [2002] data $C_{\mathrm{bdy}} = 2$ and $\hat{U}_e = 0.183$m s^{-1}.

4.2.2. Spring-Neap Variation in Tidal Range

[78] We can represent a spring-neap cycle in tidal range by prescribing a free-surface elevation of the form

$$\eta(t) = \frac{1}{2(1+\delta)}\left[1 + \delta \sin\left(\frac{t}{14}\right)\right]\cos 2t, \qquad (12)$$

where the parameter $\delta < 1$ describes the relative amplitude of the neap spring variation, and where $\hat{\eta}_0$ now represents the maximum (spring) tidal range.

[79] We can obtain C_∞ as a function of the other parameters by applying the condition

$$\lim_{x_0 \to -\infty} \int_0^{28\pi} [Q_e(U(t); x_0) - Q_d(C_\infty, U(t); x_0)]\mathrm{d}t = 0 \qquad (13)$$

as before. (This is rather cumbersome to evaluate exactly, but may be obtained to a reasonable degree of accuracy using the multiple timescales approximation described by *Pritchard* [2001]: the details are omitted here for brevity.)

[80] Figure 9 shows the deep-water concentration C_∞ as a function of U_e, for $U_e = \sqrt{2}U_d$ and $\delta = 0.25$. This is compared with the corresponding curves for a sinusoidal tidal signal of fixed range, both for $\eta(t) = \cos 2t$ (a spring tide) and for $\eta(t) = (1+\delta)^{-1}\cos 2t$ (the median tidal range). Under the spring-neap cycle, a given offshore concentration requires a higher value of U_e, and thus a lower value of $\hat{U}_0$, than under the median tide, but it requires a lower value of U_e than under the spring tide. For example, $C_\infty = 2$ requires $U_e = 0.543$ under the spring-neap cycle, $U_e = 0.67$ under the spring tide, and $U_e = 0.536$ under the median tide. This implies that the equilibrium flat which develops under a spring-neap cycle will be steeper than that associated with the median tidal range, although not as steep as that associated with the full spring tidal range. This occurs because the faster currents associated with the spring tides

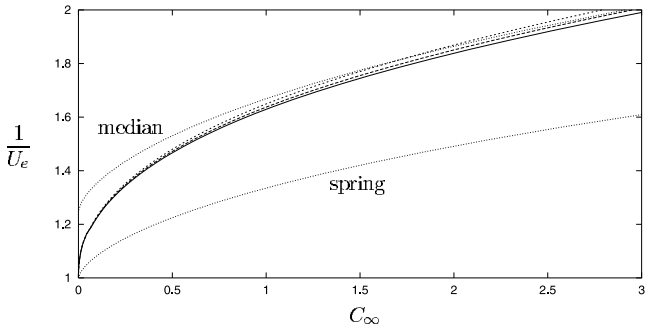

Figure 9. The quantity $1/U_e$, which is proportional to the dimensional velocity $\hat{U}_0$, plotted as a function of the dimensionless deep-water concentration C_∞ under a spring-neap cycle (see text for further details): $\epsilon = 0$ (solid lines); $\epsilon = 0.01$ (dashed lines); and $\epsilon = 0.025$ (dotted lines). The fine dotted lines represent the solution for $\epsilon = 0$ under sinusoidal tides with the median and spring ranges.

play a proportionately greater role in the sediment transport than the lower currents associated with ebb tides. However, as U_e decreases (equivalently, as C_∞ increases), the offshore concentration under the spring neap cycle approaches that under the median sinusoidal tide, because the nonlinearities in the cross-shore fluxes become relatively smaller and so the greater spring erosion and greater neap deposition tend to cancel each other out.

[81] For the parameter values considered here, we estimate a maximum current velocity of 0.337 ms^{-1} during a spring tide. In the numerical experiments of *Pritchard et al.* [2002], this is attained, although only in comparatively deep water (12 m below HW, for a spring tidal range of 7.5 m). However, this correspondence is again good enough to suggest that we have captured the essential scales of the dynamical processes when the flat is in a state of morphodynamic equilibrium.

4.3. Applications of Morphological Estimates

[82] One immediate practical application of the morphological estimates obtained here is as a baseline result when developing numerical simulations of muddy coastal systems: they can both act as a simplest scenario test case and inform the physical interpretation of numerical results.

[83] In principle, these estimates could also be tested directly by comparison with field observations. However, both empirical evidence and the results of simulations suggest that muddy shores respond to changes over a period of decades, so to compare predicted with actual change would require an observational programme on this timescale, including concurrent records of the bathymetry of a flat, the surface properties of the sediment and the offshore levels of suspended sediment, and records of extreme events such as large storms which might exert a lasting effect on the local morphology. (We note in passing the additional difficulty of judging whether estuarine environments are in an equilibrium state [*O'Connor*, 1987].)

[84] To the best of our knowledge, no data sets currently exist which satisfy these criteria. This does not mean, however, that the results described above are essentially untestable. In recent years, considerable progress has been made in developing methods to measure sediment properties in situ [see *Widdows et al.*, 1998, and references therein]; at the same time, a greater awareness of the sensitivity of coastal environments to climate change and to development has increased the incentive to carry out detailed monitoring programmes. We therefore expect that suitable observations will become available as our knowledge of these environments increases. A particularly valuable opportunity may be provided by programmes to monitor the effects of harbor engineering works that substantially change the suspended sediment regime, or affect the local tidal curve, within an estuary: an assessment of the predicted versus actual morphological change would be a useful component of such a programme, and would supply a "natural experiment" within which the ideas presented here could be thoroughly examined.

5. Summary and Conclusions

[85] We have employed a generic mathematical model to investigate the cross-shore sediment dynamics of a tidally dominated intertidal mudflat. We have obtained exact and numerical solutions for the sediment transport within our model, over two idealized bathymetries: these solutions agree in many respects with the results of more detailed numerical simulations and with field observations.

[86] The main features of these results are robust to the descriptions of sediment erosion and deposition employed. In particular, the pattern of net sediment transport is qualitatively unaffected either by introducing a secondary deposition term which represents the settling of primary particles rather than large flocs, or by modifying the dependence of the erosion rate on the excess shear stress. Between them these alternative formulations cover most of the range of empirical formulae employed to model estuarine sediment transport, and suggest that our results provide useful generic insight into the mechanisms of sediment transport over intertidal flats.

[87] In particular, our solutions provide a clear illustration of the role of settling lag in redistributing sediment across the flat. We have demonstrated several ways in which asymmetries in fluid trajectories and changes in fluid depth can contribute, through settling lag, to net transport, and indicated what signature these lag effects have in the Eulerian flux data which are directly observable in the field. Our results suggest that settling lag generally transports sediment landward; however, they raise the interesting possibility that offshore from a convex flat, settling lag may lead to the net seaward movement of sediment, rather than the net landward movement which is believed to occur in other estuarine situations. They also clarify why the criterion of uniform peak velocity across a flat, originally postulated by *Friedrichs and Aubrey* [1996], provides a good approximation to an equilibrium condition for the cross-shore profile of the flat.

[88] The other principal result of our analysis is the expression (11) which describes the suspended sediment concentration in deep water offshore from a flat, and provides a link between the short-term sediment dynamics and the large-scale morphology of the flat. This method may be used to obtain estimates for the equilibrium morphology of flats under various combinations of forcing

conditions, and allows the work of *Friedrichs and Aubrey* [1996] to be extended to provide a quantitative as well as a qualitative description of an equilibrium flat. The essential physical mechanism is that higher SSCs require generally higher velocities to sustain them, and these in turn require more gently sloping flats: this explains the strong dependence of equilibrium gradient on sediment supply found by previous numerical studies.

[89] Taken in conjunction with these numerical results, the current study provides strong evidence that the gross morphology of intertidal mudflats, and not merely their long-term erosional or accretionary behaviour, depends strongly on the external supply of sediment to the system. This is important for the design of flat regeneration schemes [*Kirby*, 2000], because it suggests that the overall scale of a rebuilt flat, as well as its bathymetry, is crucial to determining whether or not it is in an equilibrium state.

[90] Finally, while the results presented here have been obtained from a theoretical analysis of the systems in question, they raise some interesting possibilities for experimental and field investigation. In particular, they provide a testable theory for the changes in morphology which may result when the sediment supply to a muddy coast is altered (for example by engineering works), and they suggest some refinements to the theory of settling lag which is frequently invoked to explain patterns of nearshore sediment transport. Both these aspects of the work should be tested in the field in order to increase further our understanding of muddy intertidal systems.

Appendix A: Periodic Solutions for Sediment Transport

[91] We may write the Lagrangian sediment transport equation (9) as

$$\frac{\mathrm{d}C_\mathrm{L}}{\mathrm{d}t} = a(t) - b(t)C_\mathrm{L}, \quad \text{where} \quad a(t) = \frac{EQ_e(u_\mathrm{L},t)}{h_\mathrm{L}(t)}, \qquad b(t)C_\mathrm{L}(t) = \frac{EQ_d(u_\mathrm{L},t)}{h_\mathrm{L}(t)}. \tag{A1}$$

The only restrictions this places on the erosion and deposition fluxes are that Q_e is independent of C_L and Q_d is proportional to C_L: these conditions are satisfied by most empirically determined transport models, and we discuss some of these in Appendix B.

[92] When the quantities $a(t)$ and $b(t)$ are periodic with period T_1, equation (A1) has similarly periodic solutions $C_\mathrm{L}(t; x_0)$ given by

$$C_\mathrm{L}(t) = \frac{\Theta(t+T_1,t)}{1-\Omega(t+T_1,t)}, \text{ where } \Omega(t,t_0) = \exp\left(-\int_{t_0}^{t} b(t')\mathrm{d}t'\right) \tag{A2}$$

and

$$\Theta(t,t_0) = \exp\left(-\int_{t_0}^{t} b(t')\mathrm{d}t'\right)\int_{t_0}^{t}\exp\left(\int_{t_0}^{\tau} b(t')\mathrm{d}t'\right)a(\tau)\mathrm{d}\tau. \tag{A3}$$

[93] For the flows under a sinusoidal tide on a linear flat (section 3.1.1), $d(x) = -x$ and $\eta(t) = \frac{1}{2}\sin 2t$: we immediately obtain $x_\mathrm{sh}(t) = \frac{1}{2}\sin 2t$, and equation (3) then yields $U(x, t) = \cos 2t$. The depth of fluid for a given fluid element is given by $h_\mathrm{L}(t; x_0) = \eta(t) + d(x_\mathrm{L}) = \frac{1}{2}\sin 2t - \left(\frac{1}{2}\sin 2t + x_0\right) = |x_0|$, so the depth of fluid h_L is constant for any given fluid element. The period of the Lagrangian solution is then $T_1 = \frac{\pi}{2}$, half that of the Eulerian fluid motion.

[94] We construct our solutions by dividing the period of the motion into erosive, depositional and floc depositional phases. During the floc depositional phase when $|U| < U_d$, $\Omega(t, t_0)$ has the form

$$\Omega_d(t,t_0) = \exp\left\{-\frac{E}{|x_0|U_d^2}\left[\left(U_d^2 - \frac{1-\epsilon}{2}\right)(t-t_0) - \frac{1-\epsilon}{8}(\sin 4t - \sin 4t_0)\right]\right\}, \tag{A4}$$

while during the erosional and intermediate phases when $|U| \geq U_d$, it has the form

$$\Omega_e(t,t_0) = \exp\left\{-\frac{E}{|x_0|}\epsilon(t-t_0)\right\}. \tag{A5}$$

During depositional phases, $\Theta(t, t_0) = 0$, while during erosional phases $|U| > U_e$, it has the form

$$\Theta_e(t,t_0) = G(t) - G(t_0)\Omega(t,t_0), \quad \text{where}$$

$$G(t) = \frac{E^2\epsilon^2\cos 4t + 4E\epsilon|x_0|\sin 4t + \left(E^2\epsilon^2 + 16|x_0|^2\right)\left(1-2U_e^2\right)}{2U_e^2\epsilon\left(E^2\epsilon^2 + 16|x_0|^2\right)}. \tag{A6}$$

The Lagrangian solution $C_\mathrm{L}(t; x_0)$ is now given by equation (A2), where $\Theta(t, t_0)$ and $\Omega(t, t_0)$ may be expressed in terms of the quantities Θ_e, Ω_e and Ω_d with appropriate limits of integration. Finally, we substitute in $x_0 = x - \frac{1}{2}\sin 2t$ to obtain the Eulerian description $C(x, t)$, which is periodic over $0 \leq t \leq \pi$.

[95] For flow over a linear-convex flat (section 3.1.2), the Lagrangian hydrodynamic solution was constructed numerically by integrating equation (9b) forward in time using a fourth-order Runge-Kutta method [*Press et al.*, 1992]. The integrals $\Theta(t, t_0)$ and $\Omega(t, t_0)$ were then evaluated by the same method. (Computationally, it is most efficient to evaluate $C_\mathrm{L}(0)$ using equation (A2) for each fluid element, and then to integrate equation (9a) forward in time: the computation took a few tens of seconds on a Unix workstation.)

Appendix B: Alternative Erosion Formulations

[96] This paper has focused on fine cohesive sediment, for which the canonical descriptions of erosion and deposition are those due to *Einstein and Krone* [1962] and *Partheniades* [1965]. However, the analysis described here has a significantly wider application.

[97] For illustration, we consider a generalization of the sediment erosion model (5), in which the erosion flux Q_e may be written in nondimensional form as

$$Q_e = \begin{cases} \left(\dfrac{\tau}{\tau_e} - 1\right)^n & \text{for } \tau \geq \tau_e \\ 0 & \text{for } \tau < \tau_e. \end{cases} \tag{B1}$$

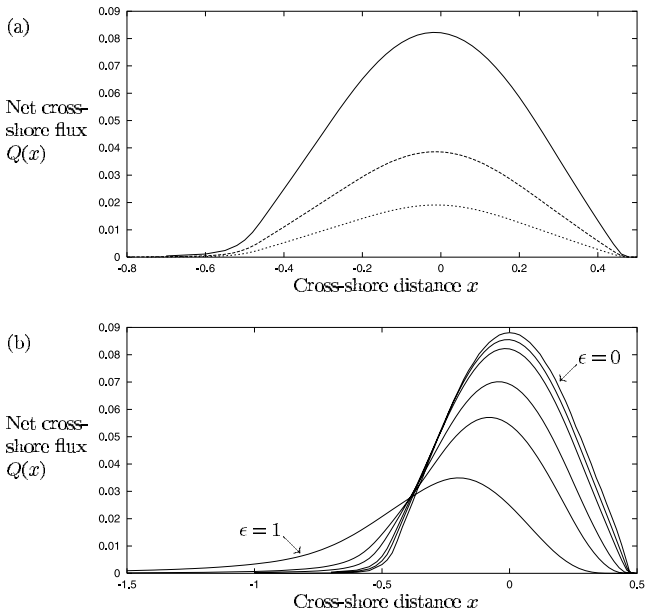

Figure B1. Residual landward sediment flux $Q(x)$ across a linear flat, for (a) $\epsilon = 0.025$ and $n = 1$ (solid line); $n = 2$ (dashed line); and $n = 3$ (dotted line); and (b) $n = 1$ and $\epsilon = 0$, 0.01, 0.025, 0.1, 0.25, and 1. Note MSL is at $x = 0$; HW and LW are at $x = \pm 0.5$.

Many standard empirical relations for sediment erosion may be approximated by choosing appropriate values for the exponent n and the critical stress τ_e. In particular, it is typical of the models used to describe the erosion of marine sands [*Dyer and Soulsby*, 1988]. Additionally, we note that by varying the quantity ϵ in equation (6), we may approximate various alternative forms of deposition: for example, $\epsilon = 1$ recovers the case of continuous deposition from a well-mixed suspension, $\hat{Q}_d = \hat{w}_s \hat{C}$, which is commonly used in studies of coarse particle transport in marine environments [see, e.g., *Schuttelaars and de Swart*, 1999].

[98] These more general cases are simple to address by the method described in Appendix A. For the flow field considered in section 3.1.1, and for integer values of n, the integrals $\Theta(t, t_0)$ and $\Omega(t, t_0)$ may be expressed in terms of elementary functions, while for noninteger n they may readily be evaluated numerically. The periodic solutions for $C(x, t)$ are very similar to those described in section 3.1.1, and so we do not present them here; however, it is instructive to investigate the variation of the cross-shore flux $Q(x)$ as the parameters n and ϵ are varied.

[99] As the exponent n is increased the erosion rate is reduced, since when U_e is sufficiently close to the maximum velocity U_0, the quantity $U^2/{U_e}^2 - 1$ is smaller than 1. Consequently, both the instantaneous equilibrium concentration C_{eq} and the deep-water concentration C_∞ are reduced. However, the main features of the concentration field and the cross-shore fluxes $q(x, t)$ are identical to those for the case $n = 1$, and the pattern of net sediment transport across the flat is unchanged (Figure B1a).

[100] As ϵ increases, continual deposition comes to dominate over shear-controlled deposition, and both the instantaneous and deep-water equilibrium concentrations are reduced. We have found that the turbid tidal edge becomes lower and less sharply pronounced, and can occur significantly further from the shoreline than when ϵ is small. (Field measurements [*Christie and Dyer*, 1998; *Christie et al.*, 1999; *Bassoullet et al.*, 2000; *Dyer et al.*, 2000a] indicate that the TTE occurs very close to the shoreline, and it is interesting that our results suggest this requires that deposition is strongly shear controlled.)

[101] A further effect is that as ϵ increases, the convergence to the offshore concentration C_∞ becomes less rapid, because the greater deposition rate leads to a greater variation in C over a tidal period. The net result of these effects can be seen in Figure B1b: the generally lower concentrations lead to a decrease in the peak flux, while the less rapid convergence to C_∞ is associated with a less rapid decay of $Q(x)$ with distance seaward.

[102] Despite the quantitative differences introduced by altering the forms of Q_e and Q_d, the overall behaviour of the solutions is remarkably consistent, especially with regard to the net cross-shore flux $Q(x)$ which is the most significant quantity for morphodynamical purposes. This strongly suggests that the processes identified here are generic features of cross-shore advective sediment transport, and so provide useful physical insight independent of the details of the empirical components of the model.

Appendix C: Robustness of Morphological Estimates

[103] As noted in section 2, the bulk properties of cohesive sediments are extremely difficult to determine in situ. Especially when they are biologically influenced, these properties may vary strongly across a flat [*Wood and Widdows*, 2002], and although the effect of spatial inhomogeneities is beyond the scope of this paper, it is useful to quantify the errors which may be introduced by such variation. While the details of such sensitivity are specific to the model we have described in this paper, they provide an indication of the inaccuracy which may be expected in any morphodynamic model, however complicated, which shares the same generic features. They therefore provide useful information about the general programme of morphodynamic modeling of mudflats.

[104] We may illustrate the sensitivity of the estimates obtained in section 4 by considering variations in $\hat{U}_e$ and $\hat{U}_d$. We suppose that one of the critical velocities $\hat{U}_e$ and $\hat{U}_d$ is known exactly, but there is some uncertainty in the other, and we wish to know how strongly this affects our estimates for $\hat{U}_0$, given a known sediment supply C_∞.

[105] This question could be addressed quantitatively by plotting C_∞ against U_d or against U_e for various values of the ratio $\hat{U}_e/\hat{U}_d$, but it is more informative to consider whether the estimate is more sensitive to an uncertainty in $\hat{U}_e$ or in $\hat{U}_d$: given the difficulty of measuring sediment properties, which is the more crucial quantity to determine accurately?

[106] This can be answered by considering the quantity $|\mathrm{d}U_e/\mathrm{d}U_d|$, when the derivatives are taken with C_∞ held constant. If this quantity is less than unity for a given value of (U_e, U_d), then a small error in U_e will have a greater effect than an equal change in U_d, and so any estimates which rely on specifying C_∞ will be more sensitive to an

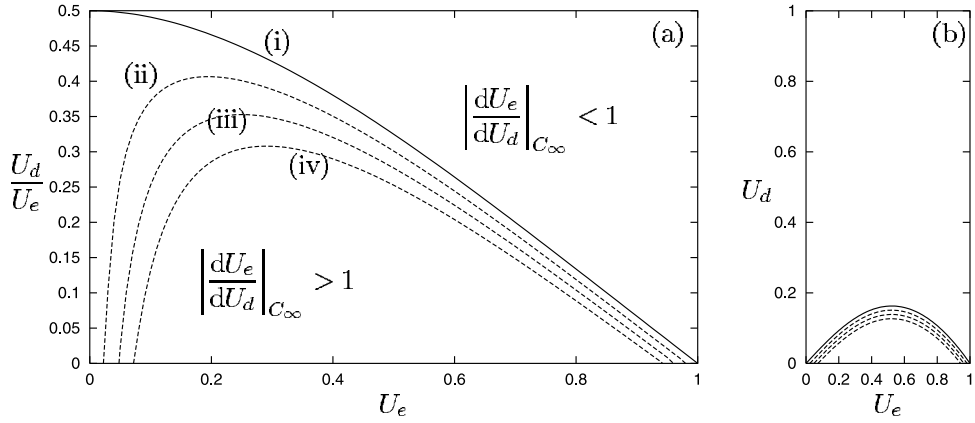

Figure C1. Regime diagrams showing where the estimate for flats gradient provided by equation (11) is more sensitive to errors in U_e than U_d (i.e., where $|dU_e/dU_d| < 1$) and vice versa. Curves represent the regime boundaries for (i) $\epsilon = 0$; (ii) $\epsilon = 0.005$; (iii) $\epsilon = 0.01$; and (iv) $\epsilon = 0.015$.

error in $\hat{U}_e$ than to one in $\hat{U}_d$. Similarly, if $|dU_e/dU_d| > 1$, the estimates will be more sensitive to errors in U_d than in U_e.

[107] Figure C1 shows the regions of (U_e, U_d) space in which our estimates are more sensitive to errors in either quantity, for a number of different values of the small parameter ϵ.

[108] For all values of ϵ, the regime in which the estimate is more sensitive to an error in $\hat{U}_d$ represents only a small part of parameter space (as Figure C1b emphasizes), and corresponds to situations in which either $\hat{U}_d$ is very much smaller than $\hat{U}_e$, or $\hat{U}_d$ and $\hat{U}_e$ are both much smaller than the critical velocity on the flat. The offshore concentrations associated with this regime are therefore extremely high. It is noteworthy that even small nonzero values of ϵ reduce this regime still further, as the particulate component of deposition comes to rival the flocculated component in magnitude, so for $\epsilon > 0$, there are values of U_e such that the estimate is always more sensitive to U_e than to U_d.

[109] We conclude that for the vast majority of flats, the value of $\hat{U}_e$ exerts more influence on the morphological estimates provided by equation (11) than the value of $\hat{U}_d$. This suggests that the development of methods to measure in situ resistance to erosion should remain the experimental priority which it has become in recent years.

[110] **Acknowledgments.** DP and AJH acknowledge financial support from EPSRC; DP also acknowledges support from HR Wallingford Ltd. (Ports and Estuaries Division) under a CASE studentship and from the Newton Trust through the BP Institute. We are grateful to Carl Friedrichs, Howell Peregrine, Bill Roberts and Giovanni Seminara, as well as to the Editors and to several anonymous reviewers, for helpful comments on various stages of this work.

References

Bassoullet, P., P. Le Hir, D. Gouleau, and S. Robert, Sediment transport over an intertidal mudflat: Field investigations and estimation of fluxes within the "Baie de Marennes-Oléron" (France), *Cont. Shelf Res.*, *20*, 1635–1653, 2000.

Brenon, I., and P. Le Hir, Modelling the turbidity maximum in the Seine estuary (France): Identification of formation processes, *Estuarine Coastal Shelf Sci.*, *49*, 525–544, 1999.

Cancino, L., and R. Neves, Hydrodynamic and sediment suspension modelling in estuarine systems. part I: Description of the numerical models, *J. Mar. Syst.*, *22*, 105–116, 1999.

Christie, M. C., and K. R. Dyer, Measurements of the turbid tidal edge over the Skeffling mudflats, in *Sedimentary Processes in the Intertidal Zone*, edited by K. Black et al., Geol. Soc., London, 1998.

Christie, M. C., K. R. Dyer, and P. Turner, Sediment flux and bed level measurements from a macro-tidal mudflat, *Estuarine Coastal Shelf Sci.*, *49*, 667–688, 1999.

Dronkers, J., Tidal asymmetry and estuarine morphology, *Neth. J. Sea Res.*, *20*, 117–131, 1986.

Dyer, K. R., *Coastal and Estuarine Sediment Dynamics*, John Wiley, Hoboken, N. J., 1986.

Dyer, K. R., The typology of intertidal mudflats, in *Sedimentary Processes in the Intertidal Zone*, edited by K. Black et al., Geol. Soc., London, 1998.

Dyer, K. R., and R. L. Soulsby, Sand transport on the continental shelf, *Annu. Rev. Fluid Mech.*, *20*, 295–324, 1988.

Dyer, K. R., et al., An investigation into processes influencing the morphodynamics of an intertidal mudflat, the Dollard Estuary, the Netherlands: I. Hydrodynamics and suspended sediment, *Estuarine Coastal Shelf Sci.*, *50*, 607–625, 2000a.

Dyer, K. R., M. C. Christie, and E. W. Wright, The classification of intertidal mudflats, *Cont. Shelf Res.*, *20*, 1039–1060, 2000b.

Einstein, H. A., and R. B. Krone, Experiments to determine modes of cohesive sediment transport in salt water, *J. Geophys. Res.*, *67*, 1451–1461, 1962.

Flemming, B. W., Geographic distribution of muddy coasts, in *Muddy Coasts of the World*, edited by T. Healy, Y. Wang, and J.-A. Healy, Elsevier, New York, 2002.

Friedrichs, C. T., and D. G. Aubrey, Uniform bottom shear stress and equilibrium hypsometry of intertidal flats, in *Mixing in Estuaries and Coastal Seas*, *Coastal Estuarine Stud.*, vol. 50, edited by C. Pattiaratchi, AGU, Washington, D. C., 1996.

Friedrichs, C. T., et al., Hydrodynamics and equilibrium sediment dynamics of shallow, funnel-shaped tidal estuaries, in *Physics of Estuaries and Coastal Seas*, edited by J. Dronkers and M. Scheffers, Balkema, Brookfield, Vt., 1998.

Groen, P., On the residual transport of suspended matter by an alternating tidal current, *Neth. J. Sea Res.*, *3*, 564–574, 1967.

Kirby, R., Effects of sea-level rise on muddy coastal margins, in *Dynamics and Exchanges in Estuaries and the Coastal Zone*, *Coastal Estuarine Stud.*, vol. 40, edited by D. Prandle, AGU, Washington, D. C., 1992.

Kirby, R., Practical implications of tidal flat shape, *Cont. Shelf Res.*, *20*, 1061–1077, 2000.

Kraus, N. C., On equilibrium properties in predictive modelling of coastal morphology change, in *Coastal Dynamics 2001*, Am. Soc. of Civ. Eng., Reston, Va., 2001.

Lee, S.-C., and A. J. Mehta, Problems in characterising dynamics of mud shore profiles, *J. Hydraul. Eng.*, *123*, 1–11, 1997.

Le Hir, P., et al., Characterization of intertidal flat hydrodynamics, *Cont. Shelf Res.*, *20*, 433–459, 2000.

Nichols, M. M., and R. B. Biggs, Estuaries, in *Coastal Sedimentary Environments*, edited by R. Davis, pp. 136–139, Springer-Verlag, New York, 1985.

O'Connor, B. A., Short and long term changes in estuary capacity, *J. Geol. Soc. London*, *144*, 187–195, 1987.

Partheniades, E., Erosion and deposition of cohesive soils, *J. Hydraul. Eng.*, *91*, 105–139, 1965.

Peregrine, D. H., Equations for water waves and the approximations behind them, in *Waves on Beaches and Resulting Sediment Transport*, edited by R. Meyer, Academic, San Diego, Calif., 1972.

Postma, H., Transport and accumulation of suspended matter in the Dutch Wadden Sea, *Neth. J. Sea Res.*, *1*, 148–190, 1961.
Press, W. H., et al., *Numerical Recipes in Fortran* 77, 2nd ed., Cambridge Univ. Press, New York, 1992.
Pritchard, D., Some problems in two-phase flow, Ph.D. thesis, Univ. of Bristol, Bristol, U. K., 2001.
Pritchard, D., A. J. Hogg, and W. Roberts, Morphological modelling of intertidal mudflats: The role of cross-shore tidal currents, *Cont. Shelf Res.*, *22*, 1887–1895, 2002.
Roberts, W., and R. J. S. Whitehouse, Long-term morphodynamic modelling of intertidal mudflats, *Rep. TR 48*, HR Wallingford Ltd., Oxfordshire, U.K., 1997.
Roberts, W., P. Le Hir, and R. J. S. Whitehouse, Investigation using simple mathematical models of the effect of tidal currents and waves on the profile shape of intertidal mudflats, *Cont. Shelf Res.*, *20*, 1079–1097, 2000.
Sanford, L. P., and J. P. Halka, Assessing the paradigm of mutually exclusive erosion and deposition of mud, with examples from upper Chesapeake Bay, *Mar. Geol.*, *114*, 37–57, 1993.
Sanford, L. P., and J.P.-Y. Maa, A unified erosion formulation for fine sediments, *Mar. Geol.*, *179*, 9–23, 2001.
Schuttelaars, H. M., and H. E. de Swart, Initial formation of channels and shoals in a short tidal embayment, *J. Fluid Mech.*, *386*, 15–42, 1999.
van Straaten, L. M. J. U., and P. H. Kuenen, Tidal action as a cause of clay accumulation, *J. Sediment. Petrol.*, *28*, 406–413, 1958.
Wang, B. C., and D. Eisma, Supply and deposition of sediment along the north bank of Hangzhou Bay, China, *Neth. J. Sea Res.*, *25*, 377–390, 1990.
Widdows, J., et al., A benthic annular flume for in situ measurements of suspension feeding/biodeposition rates and erosion potential of intertidal cohesive sediments, *Estuarine Coastal Shelf Sci.*, *46*, 27–38, 1998.
Winterwerp, J. C., On the flocculation and settling velocity of estuarine mud, *Cont. Shelf Res.*, *22*, 1339–1360, 2002.
Wood, R., and J. Widdows, A model of biotically-influenced sediment transport over an intertidal transect, comparing the influences of biological and physical factors, *Limnol. Oceanogr.*, *47*, 848–855, 2002.

A. J. Hogg, Centre for Environmental and Geophysical Flows, Department of Mathematics, University of Bristol, University Walk, Bristol BS8 1TW, UK. (a.j.hogg@bristol.ac.uk)
D. Pritchard, B. P. Institute for Multiphase Flow, University of Cambridge, Madingley Rise, Cambridge CB3 0EZ, UK. (david@bpi.cam.ac.uk)